Supporting Information:

Phenoxazine-based Small Molecule Heterojunction Nanoparticles for Photocatalytic Hydrogen Production

Mariia V. Pavliuk,[§] Sina Wrede,[§] Haining Tian*[,§]

§Department of Chemistry - Ångström Laboratory, Physical Chemistry, Uppsala University, 751 20 Uppsala, Sweden

Table of Content	Page
I. Materials and Methods	S3
II. Synthesis and characterization of POZ-M	S6
Figure S1. HR-ESI-MS(nanoSpray) data for POZ-M	S6
Figure S2. ^{1}H NMR spectra for POZ-M in $CDCl_3$.	S7
Figure S3. ^{13}C NMR spectra for POZ-M in $CDCl_3$.	S7
Figure S4. Distribution of the hydrodynamic diameter of POZ-M, ITIC and POZ-M:ITIC NPs	S8
Figure S5. Powder X-ray diffraction (PXRD) patterns of small molecules composed of POZ-M, ITIC, and PXRD pattern of lyophilized POZ-M:ITIC heterojunction NPs	S8
Figure S6. Cryo-TEM micrographs of POZ-M:ITIC NPs without and with photodeposited Pt	S9
Figure S7. Differential pulse voltammograms of POZ-M	S9
Table S1. Redox potentials vs. NHE	S9
Figure S8. Normalized steady-state UV-Vis absorption spectra for small molecule POZ-M NPs, POZ-M:ITIC NPs in water and POZ-M in THF.	S10
Figure S9. Photoluminescence spectra under excitation of 495 nm and 640 nm for POZ-M NPs, ITIC NPs and POZ-M:ITIC NPs with various ratios	S10
Figure S10. The fluorescence excitation spectrum of POZ-M:ITIC NPs with emission at 870nm.	S10
Figure S11. Steady state PL spectra of heterojunction and mixed NPs upon excitation at 495 nm. The fluorescence excitation spectrum recorded for mixed NPs with emission at 870 nm.	S11
Figure S12. TA data for single molecules ITIC NPs and POZ-M NPs.	S11
Figure S13. TA dynamics extracted for heterojunction NPs under deafferent excitation powers	S12

I. Materials and Methods.

Materials. Reagents were purchased from either Sigma Aldrich (n-type non-fullerene small molecule 2,2′-[[6,6,12,12-Tetrakis(4-hexylphenyl)-6,12-dihydrodithieno[2,3-d:2′,3′-d′]-s-indaceno[1,2-b:5,6-b′]dithiophene-2,8-diyl]bis[methylidyne (3-oxo-1H-indene-2,1(3H)-diylidene)]]bis[propanedinitrile, coded as **ITIC**); or Polymer Source Inc., Canada (the copolymer polystyrene grafted with carboxy terminated polyethylene oxide, coded as **PEG**, backbone chain Mw 8500, graft chain Mw 4600, total chain Mw 36 500), except for **POZ-M** which was synthesized using a synthetic procedure described in Supporting information. The centrifuge tubes with molecular weight (Mw) cutoffs of 10 kDa (Amicon Ultra-15) were purchased from Sigma-Aldrich. The syringes filters with PVDF (polyvinylidene difluoride) membrane and 0.45μm pore size have been purchased from PALL (Pall corporation). Tetrahydrofuran (THF) was purchased from VWR Chemicals. All the chemicals were used without any further filtration or purification unless stated otherwise.

Preparation of Small Molecule Organic Nanoparticles. NPs were synthesized using a modified nanoprecipitation method. At first, POZ-M (1 mg/mL), ITIC (5 mg/mL), and PEG (4.5 mg/mL) were dissolved in THF and sonicated (5 min for POZ-M, ITIC, or 25 min for PEG) to prepare stock solutions. Then the stock solutions were mixed in different ratios with addition of THF in order to obtain the desired POZ-M:ITIC:PEG NPs composition as 1:1:2 or1:2:2 (V_{total} = 500 μL). These mixtures were sonicated for ten minutes and then injected fast to a separate vial with 12 mL of deionized water. Resulting solutions were covered with an aluminum foil to avoid exposure of light, and were sonicated for additional 6-9 min. Afterwards the mixtures were left in fume hood until complete THF evaporation. Resulting NPs were filtered with a 0.45 μm syringe filter, and then concentrated using centrifuge. The final concentration of organic molecules in NPs was determined by analyzing the absorbance spectra of the freeze-dried NPs redissolved in THF.

General methods. The hydrodynamic diameters of small molecule NPs were conducted on a Zetasizer Nano S (Malvern, U.K). Power X ray diffraction has been collected with a step of 0.02° from 4° to 60° on Simons D5000 diffractometer (Cu Kα, λ= 0.15418 nm) at 45 KV and 40 mA. ^{1}H NMR and ^{13}C NMR spectra of POZ-M were recorded in $CDCl_3$ on a JEOL resonance 400 MHz spectrometer. UHPLC method: The sample was dissolved in THF. UHPLC Agilent InfinityLab LC/MSD series 6100 system using an Agilent InfinityLab Poroshell 120 SB-C18 3 mm × 50 mm, 2.7 μm HPLC column with HPLC grade water (0.1% formic acid): UHPLC grade CH3CN eluent system using the method: 0–1 min: iso 10% CH_3CN, 1–10 min: 10%→90% CH_3CN, 10–11 min: iso 90% CH_3CN, 11–12 min: 90%→10% CH3CN, flow rate: 1 mL/min; UV- (1260 Infinity II Diode Array Detector HS). The sample was dissolved $CHCl_3$:MeOH 1:1 for HR-ESI-MS analyses. HR-ESI-MS analyses were performed at the Organisch Chemisches Institut WWU Münster, Germany.

Cryo-Transmission Electron Microscopy (Cryo-EM) has been performed on a Zeiss Libra 120 transmission electron microscope (Carl Zeiss AG, Oberkochen, Germany) operating at 80 kV and in zero-loss bright-field mode. Low-dose conditions with a BioVision Pro-SM Slow Scan CCD camera (Proscan Elektronische Systeme GmbH, Scheuring, Germany) were used to obtain digital images. R1.3/1.2 200 and 300 mesh grids (QuantiFoil) were glow-discharged (20 mA for 120 s) on a PELCO EasiGlow. Concentrations of NPs were as following: ITIC (346 μg/mL), POZ-M:ITIC (300 μg/mL). Each mixture (3 μL) was applied onto grids before plunge-freezing into liquid ethane in a Vitroblot Mark IV robot (FEI/Thermo Fisher Scientific) operating at 25 °C, 95% humidity (blot time of 4 or 6 s). Samples were vitrified in liquid ethane and transferred to the microscope, continuously kept below –160 °C and protected against atmospheric conditions.

The UV-Vis absorption spectra of the synthesized NPs were acquired using a Varian Cary 50. The steady-state fluorescence and excitation spectra have been measured on Flurolog iHR 320 (Horiba Jobin Yvon) using the Fluoracle software (the absorbance of NPs was adjusted to 0.05 a.u.). Quantum yields were acquired using Rhodamine 6G as reference. Both steady-state absorption and fluorescence spectra were recorded in quartz cuvettes.

Differential pulse voltammetry measurements were measured with a step size of 5 mV, modulation amplitude of 25 mV and interval time of 0.5 s (giving a scan rate of 10 mV/s). The experiments were carried out by dissolving the small molecules in dried tetrahydrofuran (THF) with 0.1 M tetrabutylammonium hexafluorophophate, $TBAPF_6$, (Sigma-Aldrich, electrochemical grade, dried at 80 °C in a vacuum) and purged with solvent-saturated argon or in 0.1 M KCl aqueous solution. Differential pulse voltammograms were recorded in a cylindrical standard three-electrode cell using an Autolab potentiostat (PGSTAT302N, Metrohm, Switzerland) controlled with NOVA software. As electrodes, a non-aqueous silver reference electrode for measurements in THF or an aqueous Ag/AgCl reference electrode filled with 4 M KCl, platinum wire counter electrode and a 3 mm diameter glassy carbon disc electrode as working electrode were used. The glassy carbon electrode was polished with a 0.05-micron Al paste on a polishing pad. Ferrocene with a potential versus the normal hydrogen electrode (NHE) value of +0.63 V vs NHE was added as an internal redox standard at the end of each experiment in THF. For conversion of the aqueous Ag/AgCl reference, a value of +0.195 V vs NHE was used from calibration.

Transient Absorption Spectroscopy. To generate the pump and probe (super continuum), the output of a 3 kHz Ti:Sapphire amplifier (1.5 mJ, 45 fs FWHM, Libra, Coherent) was split. The 495 and 640 nm excitation light was obtained by directing the pump beam into the optical parametric amplifier, TOPAS-White/ TOPAS-Prime, and TOPAS SHS/TOPAS NirVis (Light Conversion). The output was passed through a mechanical chopper, blocking every second pulse, and was focused onto the sample.

The pump intensity was attenuated to 60-500 μW. The probe was optically delayed (≤8 ns, Newport) and converted into a white light supercontinuum with a vertically moving, 4 mm CaF_2 crystal. The probe light was detected by a custom-made 200-1000 nm silicon diode array (Newport). For each sample, 3 to 6 scans were averaged of 1500 ms integration each. Surface Xplorer was used to autocorrect for pump scattering. The kinetic traces were fitted as a sum of convoluted exponentials. Mdots samples were prepared in quartz cuvettes (1 mm × 10 mm path length) and the absorbance of all samples was adjusted to 0.6. Spectra of the oxidized or reduced species were recorded for the dissolved molecules in 0.1 M $TBAPF_6$ (in dry THF, purged with solvent saturated argon) recorded with a diode array spectrophotometer (Agilent 8453). The measurements were carried out in a thin-layer quartz cuvette spectroelectrochemical cell with a platinum minigrid working electrode, platinum wire counter electrode and non-aqueous silver reference electrode. A potential 200 mV lower than the reduction potential or higher of the oxidation potential was applied as potential step.

Photocatalytic studies. The photocatalytic experiments were performed in a gastight vials (total volume 9 mL). At first solution of small molecule organic NPs was mixed with the aqueous potassium hexachloroplatinate solution and purged with Ar (99.99 % pure) for 20 min (10 min inside the solution and 10 min above solution). Afterwads 0.2 M ascorbic acid was introduced and resulting mixture was purged for additional 20 min above the solution. Photocatalytic mixtures were illuminated with LED PAR38 lamp (17W, 50 mW cm^{-2}, 420-750 nm), and the produced hydrogen was measured using gas chromatography (PerkinElmer LLC, MA). After each removal of hydrogen from the headspace, the top of gastight vials was covered with Play-Doh (Hasbro Inc). All experiments were repeated in triplicates.

II. Synthesis and characterization of POZ-M (5,5'-(10-octyl-10H-phenoxazine-3,7-diyl)-bis(thiophene-2-carbaldehyde)

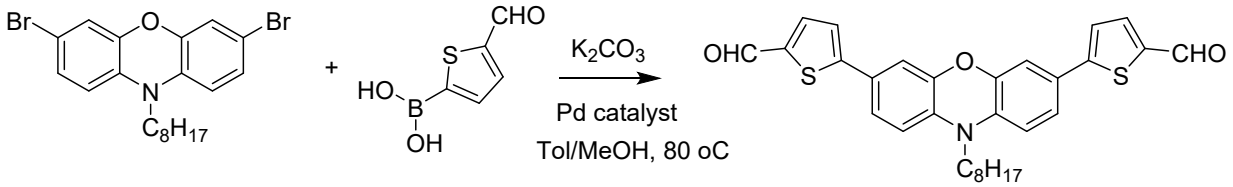

POZ-2Br **POZ-M**

POZ-2Br (0.45 g, 1 mmol), (5-formylthiophen-2-yl)boronic acid (0.35 g, 2.25 mmol), potassium carbonate (1.1 g, 7.5 mmol) and [1,1'-Bis(diphenylphosphino)ferrocene]-dichloropalladium(II) (0.11 g, 7.5 mmol) were mixed in 5 ml of toluene(Tol)/methanol(MeOH) 1:1 (v/v) and then placed in a sealable tubes. The mixture was degassed with N_2 and stirred at 80°C for 3,5h. Then the reaction solution was mixed with 15 ml of water and was extracted with dichloromethane (DCM) to give the crude product.

Column purification with silica gel and DCM/MeOH 30:1 (v/v) gave the final product **POZ-M** as red powder (0.350 g, 68 %). ^{1}H NMR (400 MHz, in $CDCl_3$): δ = 7.68 (d, *J* = 3.9Hz, 1H), 7.23 (d, *J* = 3.9 Hz, 1H), 7.13 (dd, *J* = 8.3, 2.1 Hz, 1H), 6.92 (d, *J* = 2.0 Hz, 1H), 6.49 (d, *J* = 8.4 Hz, 1H), 3.50 (t, *J* = 8.1Hz, 1H), 0.92-0.87 (m, 1H). ^{13}C NMR (101 MHz, $CDCl_3$) δ ppm, 182.70, 153.63, 144.89, 141.36, 137.82, 133.62, 126.47, 122.91, 122.46, 113.18, 111.93, 44.37, 31.90, 29.47, 29.40, 27.01, 25.21, 22.76, 14.23. HR-ESI-MS(nanoSpray): M = $C_{30}H_{29}NO_3S_2$, $(M+H)^+$ found 516.16648 (calculated 516.16616); $(M+Na)^+$ found 538.14827 (calculated 538.14811)

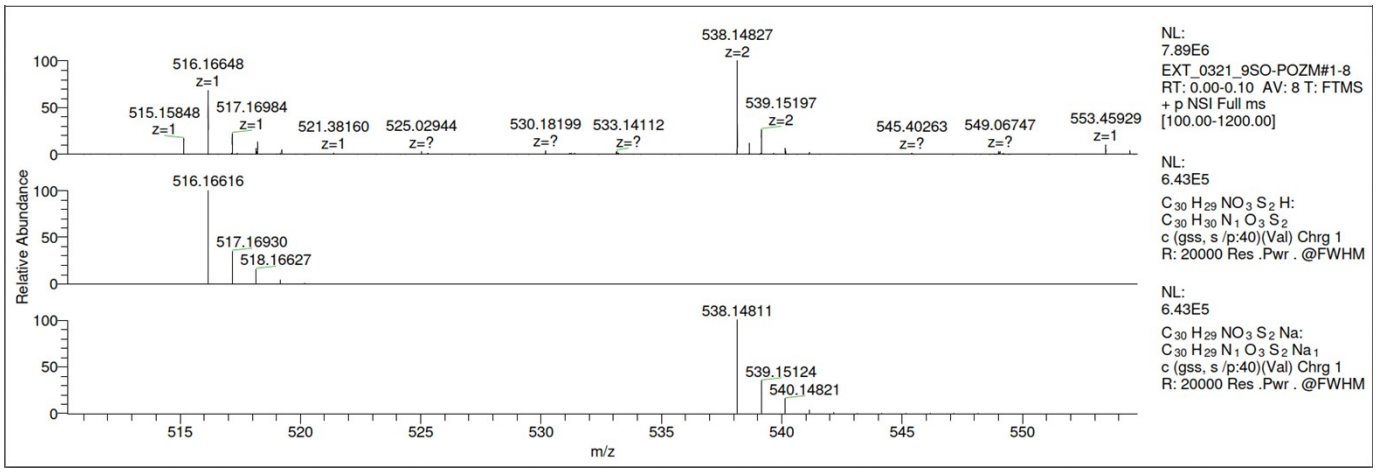

Figure S1. HR-ESI-MS(nanoSpray) data for POZ-M.

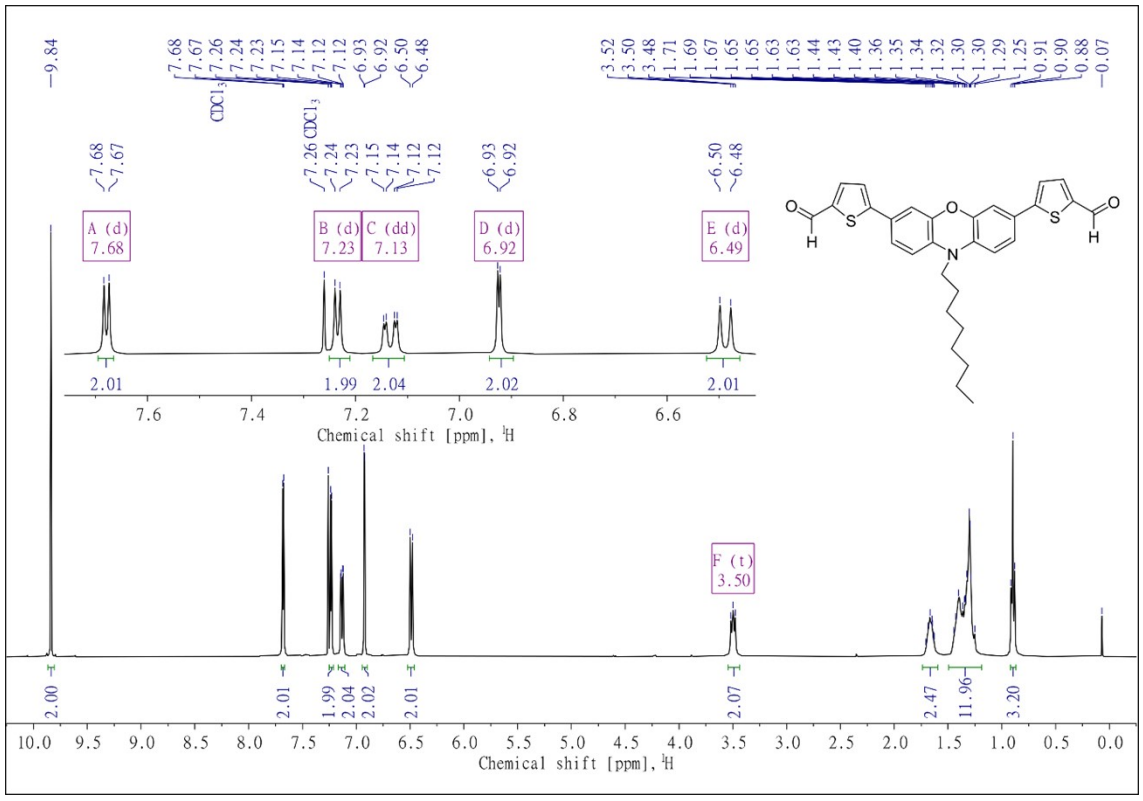

Figure S2. ^{1}H NMR spectra for POZ-M in $CDCl_3$.

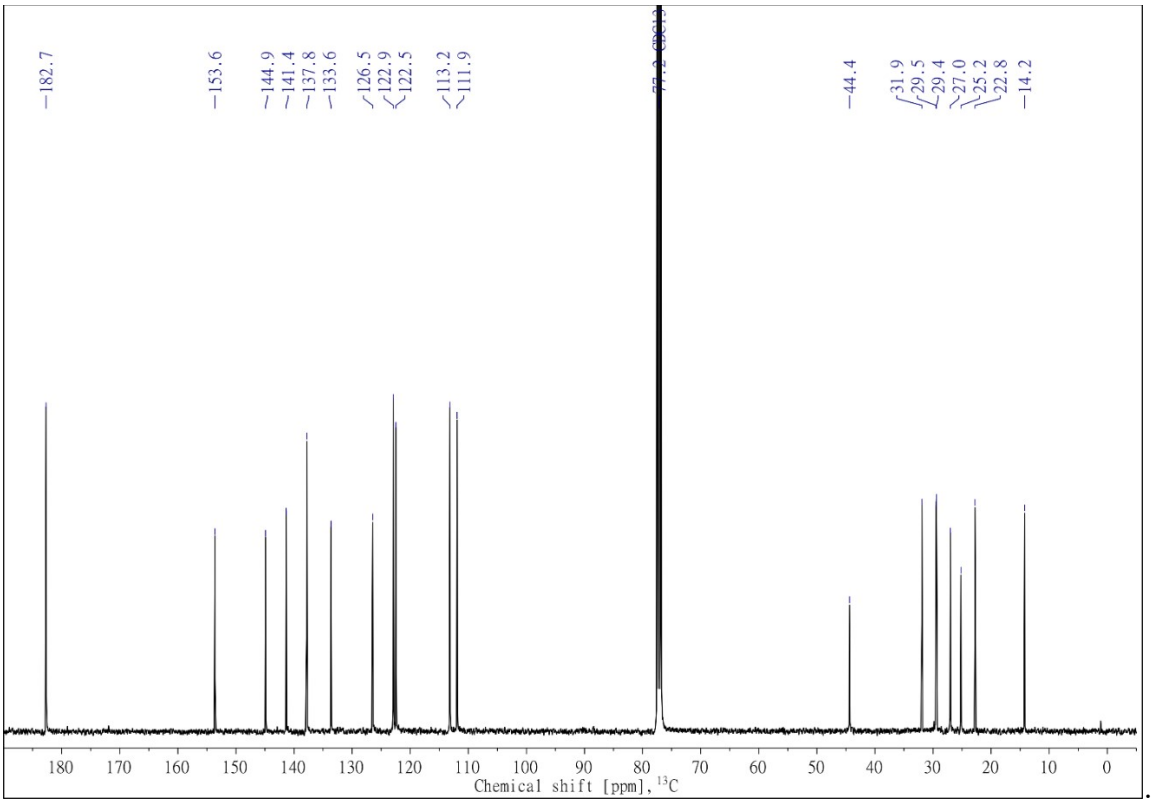

Figure S3. ^{13}C NMR spectra for POZ-M in $CDCl_3$.

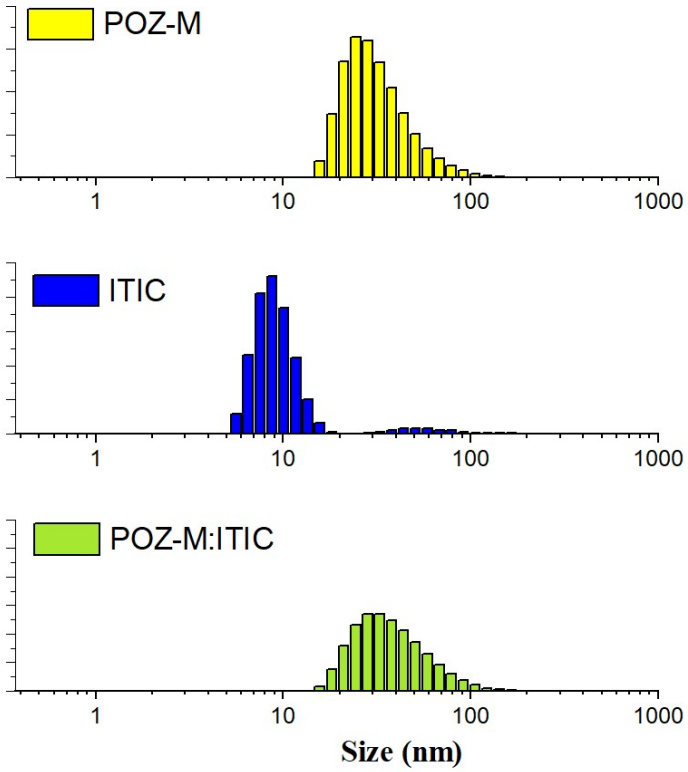

Figure S4. Distribution of the hydrodynamic diameter of POZ-M, ITIC and POZ-M:ITIC nanoparticles

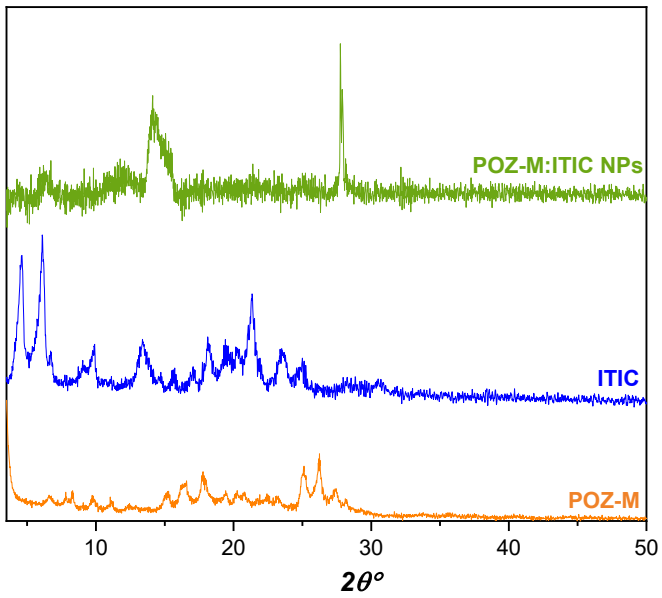

Figure S5. Powder X-ray diffraction (PXRD) patterns of small molecules POZ-M (orange line), ITIC (blue line), and PXRD pattern of lyophilized POZ-M:ITIC heterojunction POZ-M:ITIC NPs (green line)

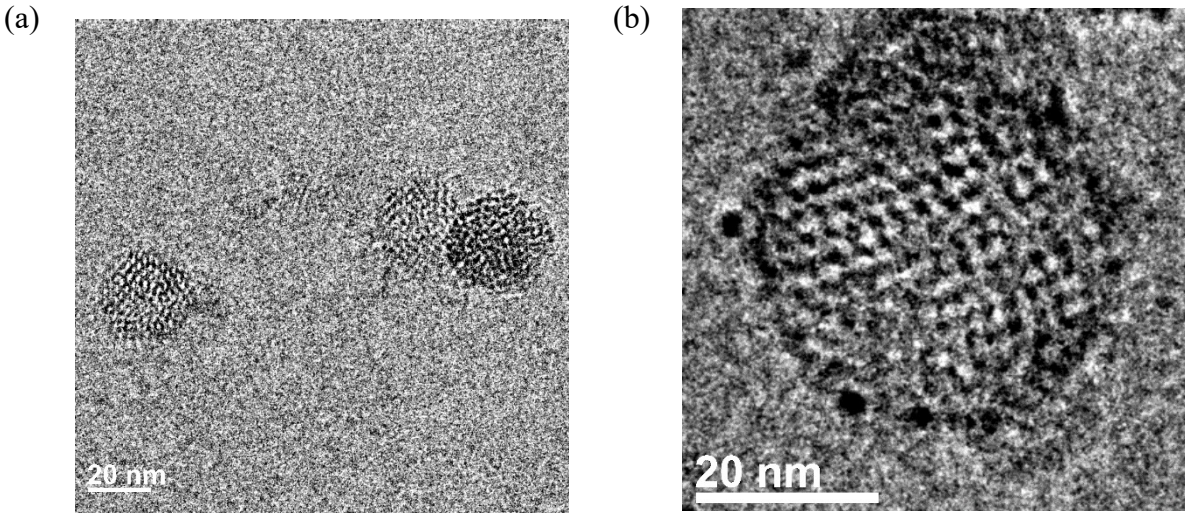

Figure S6. Cryo-TEM micrographs of small molecule NPs without (a, before photocatalysis) and with photodeposited Pt (b, after photocatalysis).

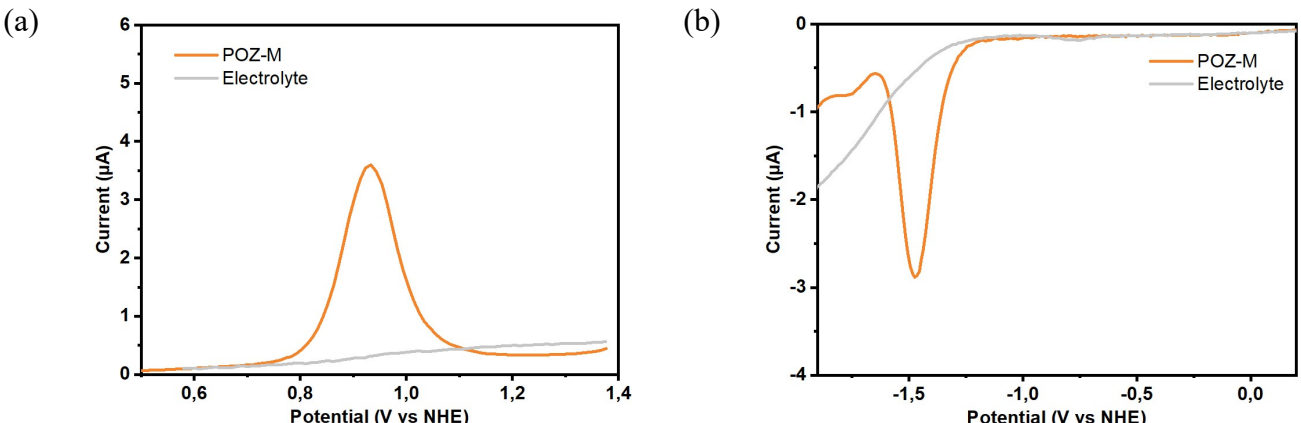

(c)

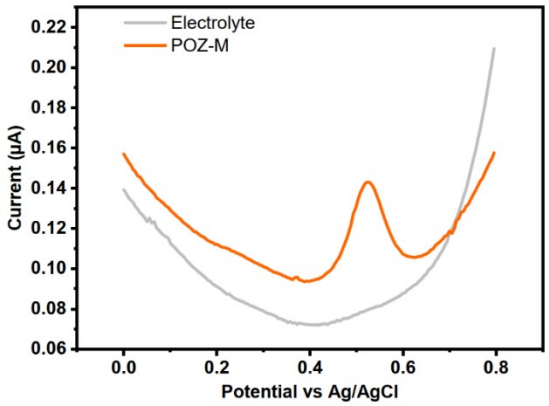

Figure S7. (a, b) Differential pulse voltammograms of POZ-M dissolved in 0.1 M $TBAPF_6$ in THF. (c) Differential pulse voltammograms of POZ-M NPs in 0.1 M KCl aqueous solution.

Table S1. Redox potentials of POZ-M vs. Normal Hydrogen Electrode (NHE)

Sample	Solvent	$E_{0\text{-}0}$ (eV)	$E_{POZ\text{-}M\text{-}/POZ\text{-}M}$ (V vs NHE)	$E_{POZ\text{-}M/POZ\text{-}M+}$ (V vs NHE)	$E_{POZ\text{-}M\text{-}/POZ\text{-}M^*}$ (V vs NHE)	$E_{POZ\text{-}M^*/POZ\text{-}M+}$ (V vs NHE)
POZ-M	THF	2.42	-1.47	0.93	0.95	-1.49
POZ-M NPs	H_2O	2.24	N/A	0.72	N/A	-1.52

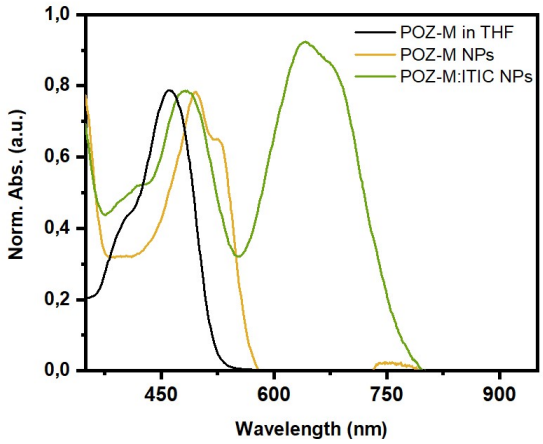

Figure S8. Normalized steady-state UV-Vis absorption spectra for small molecule POZ-M NPs (orange), POZ-M:ITIC NPs (green) in water and POZ-M in THF (black).

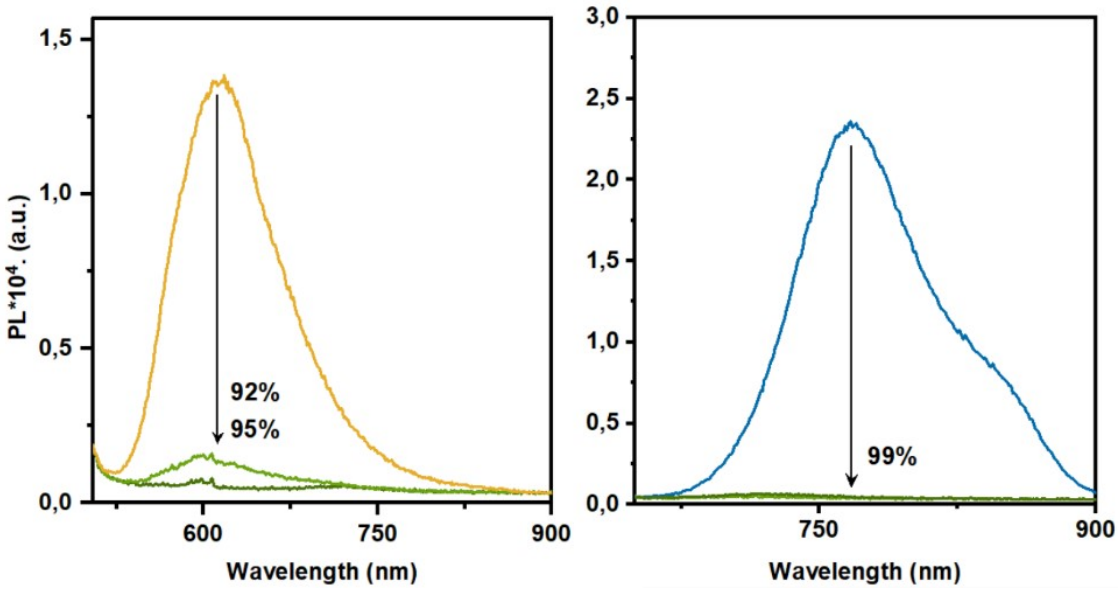

Figure S9. Photoluminescence spectra under excitation of 495 nm and 640 nm for POZ-M NPs (orange line), ITIC NPs (blue line) and POZ-M:ITIC NPs with ratio of 1:1 (light green line) and 1:2 (dark green line). For photoluminescence studies absorption of all samples was normalized to 0.05.

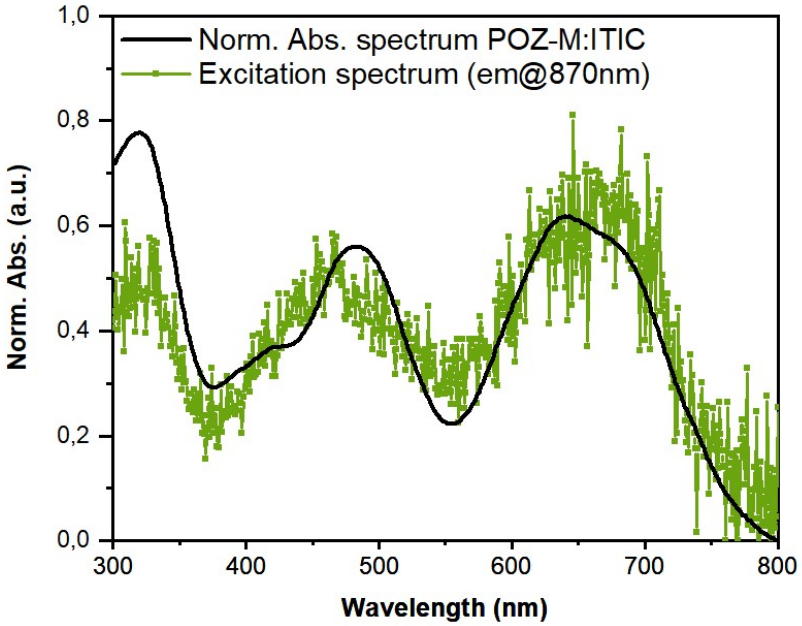

Figure S10. The fluorescence excitation spectrum of POZ-M:ITIC heterojunction NPs with emission at 870 nm.

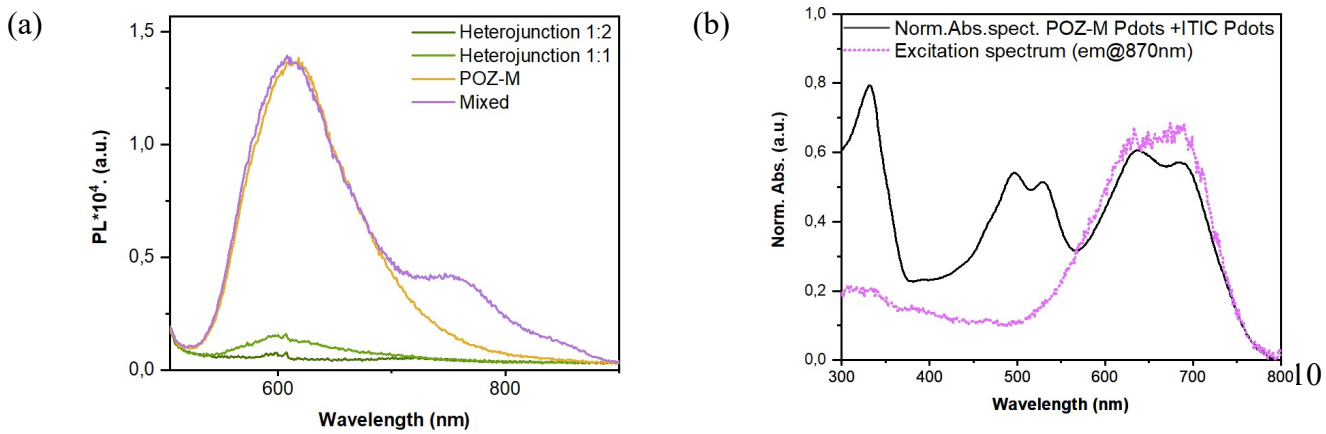

Figure S11. (a) Steady state PL spectra of POZ-M NPs (orange line), heterojunction POZ-M:ITIC NPs (green and dark green lines for 1:1 and 1:2 ratios respectively), and POZ-M NPs and ITIC NPs mixed together upon excitation at 495 nm (purple line). (b) Normalized steady-state UV–vis (black) of mixed POZ-M NPs and ITIC NPs. The fluorescence excitation spectrum recorded for mixed NPs with emission at 870 nm (purple line).

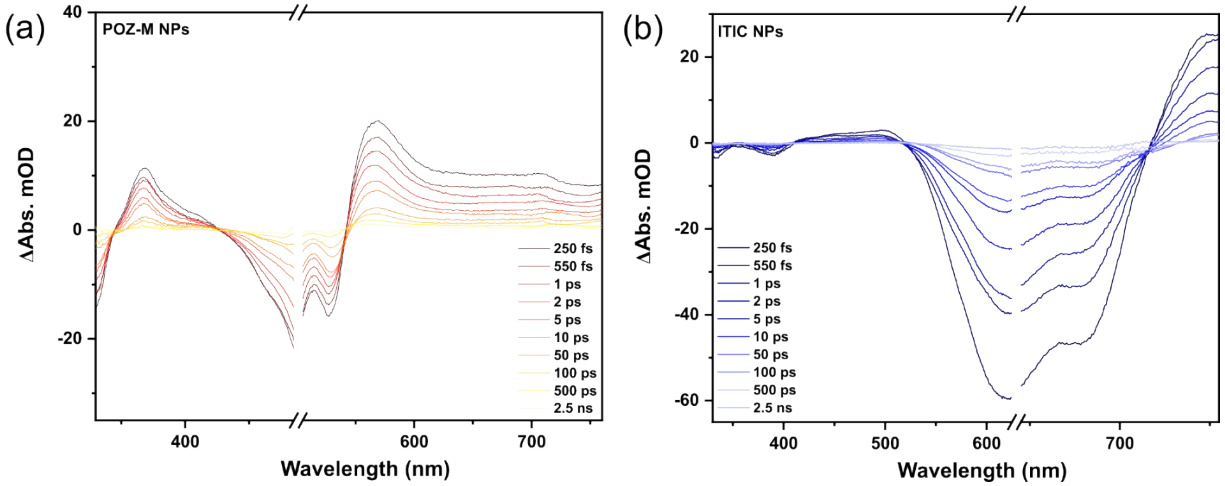

Figure S12. TA data for single molecules ITIC (a) and POZ-M (c), recorded in THF under excitation of 640 and 495 nm respectively. TA data for ITIC NPs (b) and POZ-M NPs (d) excited at 640 and 495 nm respectively. Analysis of charge generation dynamics began from assignment and characterization of TA data for single molecule POZ-M NPs and ITIC NPs pumped at 495 and 640 nm respectively We note a distinct photoinduced bleaching (GSB) at 500 nm and a positive signal extending from 570 to 750 nm (ESA, excited state absorption) in POZ-M NPs, accordant with its steady-state absorption peak. Based on earlier reports on ITIC, the negative signal at 500 nm and positive signal extending from 570 to 750 nm of ITIC NPs were assigned to GSB and ESA respectively. Eventually, for the ITIC NPs we observed rapid decay of GSB and ESA, due to the recombination of singlet excitons to the ground state within their lifetime.

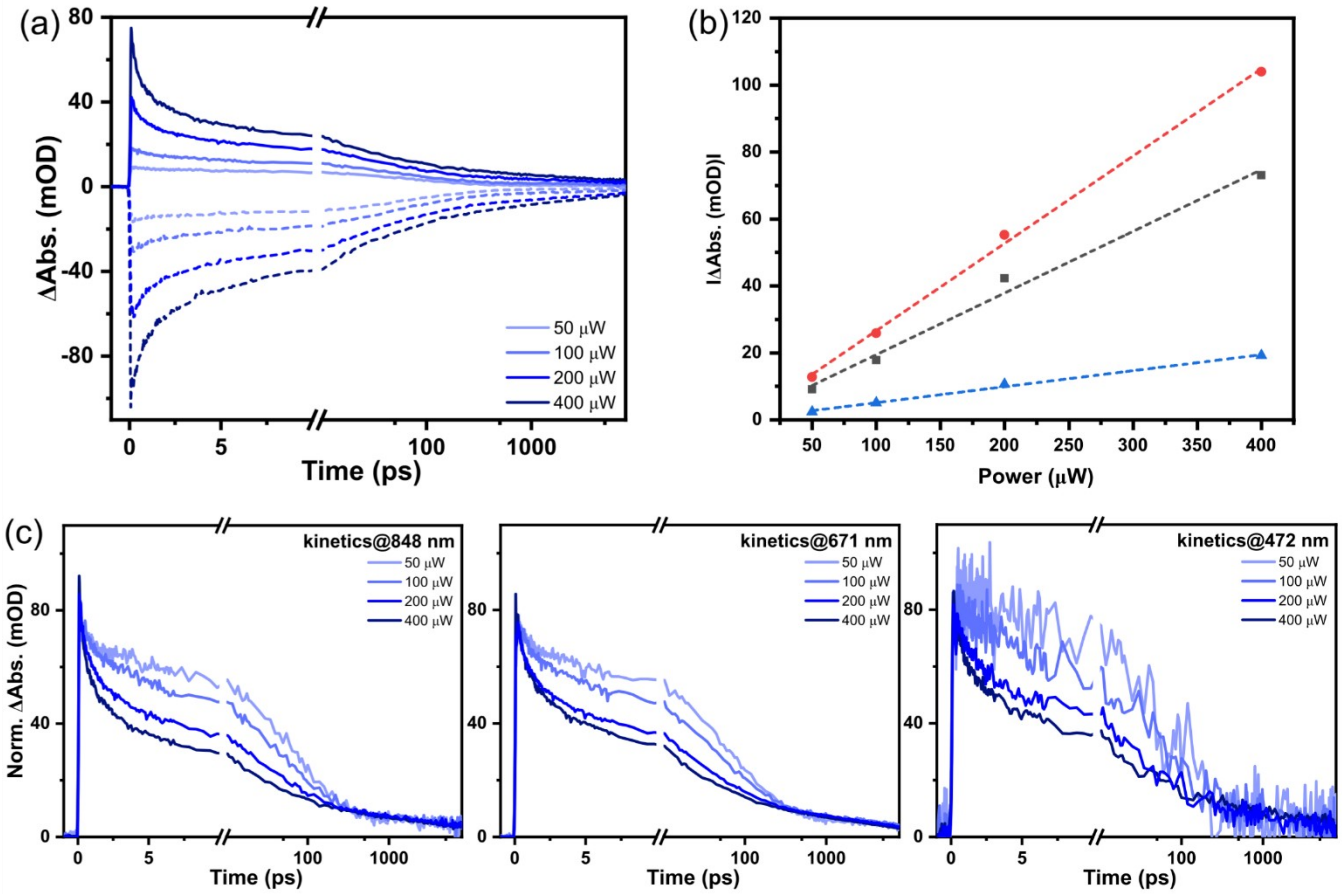

Figure S13. TA dynamics extracted for heterojunction NPs under deafferent excitation powers ($\lambda_{exc.}$ 640 nm). (a) non-normalized kinetics, (c) normalized kinetic traces extracted at 850 nm, 670 nm and 470 nm. (b) Dependence of TA amplitude at 850 nm (black dashed line), 670 nm (red dashed line), and 470 nm (blue dashed line) versus different excitation powers. Normalized TA dynamics within POZ-M:ITIC NPs at 470, 670 and 850 nm under excitation powers ranging from 50 μW to 400 μW is presented in Figure S10. At higher pump powers, faster decay processes dominate transient dynamics as evident from the increased amplitude of an additional deactivation pathway, namely singlet-singlet exciton annihilation (SSA, τ<1 ps). Thus, the decay dynamics were further studied at the lowest possible excitation powers with decent signal to noise ratio.

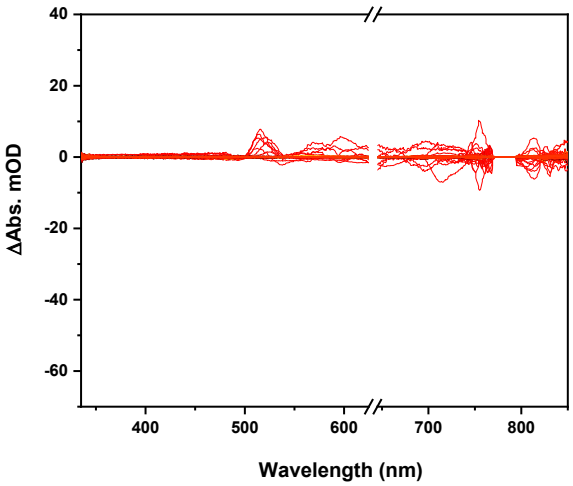

Figure S14. TA data for POZ-M NPs under excitation of 640 nm

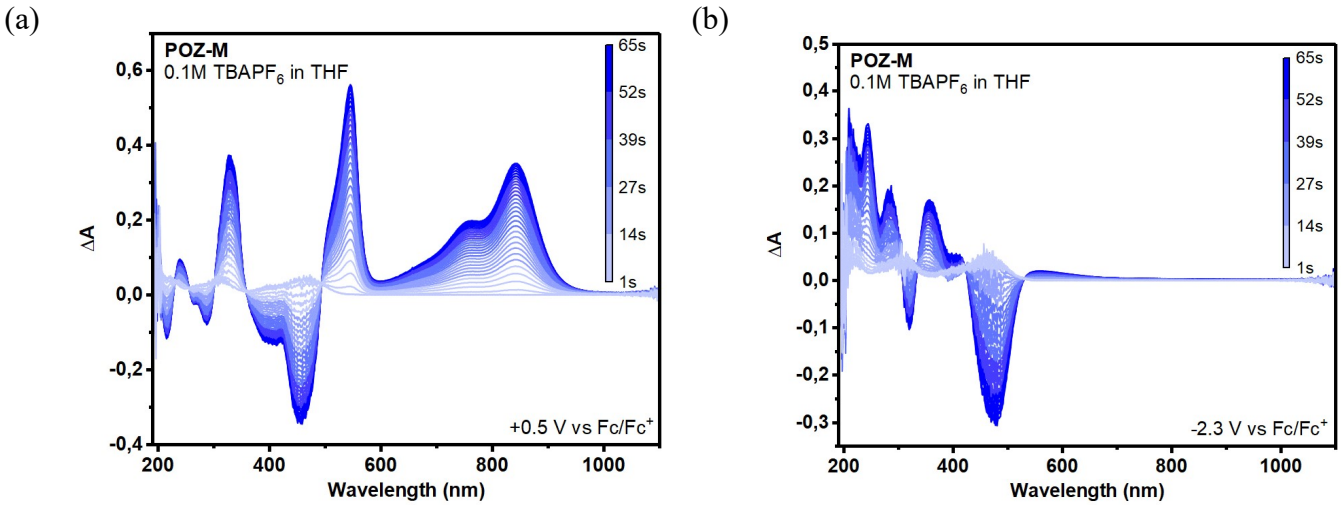

Figure S15. Spectroelectrochemistry data collected for small molecule POZ-M in THF. Corresponding UV-Vis spectra of oxidized POZ-M molecule (a, collected at 0.5 V vs Fc/Fc^{+}), reduced POZ-M molecule (b, collected at -2.3 V vs Fc/Fc^{+}).

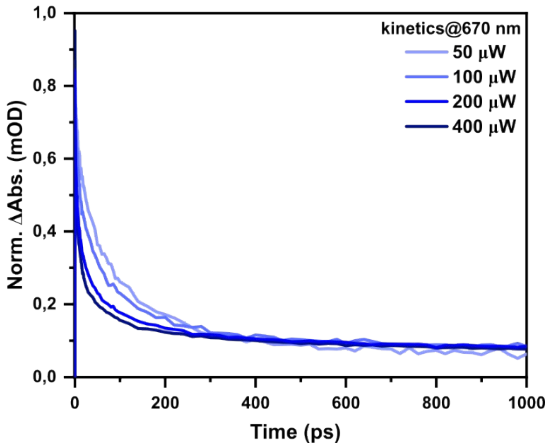

Figure S16. Kinetic traces extracted at 670 nm for POZ-M:ITIC heterojunction NPs excited at different excitation powers (50-400 µW, $\lambda_{exc.}$ 640 nm). TA kinetics at 670 nm for POZ-M:ITIC recorded at the lowest excitation power tend to level off after 200 ps. This indicate that there is almost no recombination loss even in the absence of catalyst or ascorbic acid, when the HT is complete in heterojunction NPs.

III. TAS for POZ-M/ITIC NPs under 495 nm excitation

Upon excitation at 495 nm, 90 % of photons are absorbed by POZ-M and 10 % of photons are absorbed by ITIC. The transient signals of heterojunction NPs under 495 nm excitation are different from single molecule ITIC NPs or POZ-M NPs, and rather resemble transient signals for POZ-M:ITIC under 640 nm excitation. TA spectra and the normalized dynamics for POZ-M:ITIC NPs, POZ-M NPs and ITIC NPs extracted at 670 nm are shown in **Figure S15**. The strong GSB at 670 nm persists to the long delay time, suggesting the formation of long-lived charge-separated state, similarly to TA data results obtained under 640 nm excitation. TA signals for heterojunction NPs centered from 400 to 500 nm (**Figure S15b**, $\lambda_{exc.}$ 495 nm) immediately after excitation (τ< 200 fs) resemble the signals for heterojunction NPs excited at 640 (**Figure 3**, main text), where efficient hole transfer from ITIC* to POZ-M occurs, rather than TA signals from the GSB of POZ-M (**Figure S15c**). Thus, we speculate that HT dominates the TA dynamics of heterojunction NPs under 495 nm excitation. As we know about the contribution of EnT from steady state measurements, we suggest that EnT from POZ-M* to ITIC, followed by fast HT from ITIC* to POZ-M are the main photophysical processes in POZ-M:ITIC NPs. However, direct ET from POZ-M* to ITIC shouldn't be excluded based on sufficient thermodynamic driving force (0.89 V).

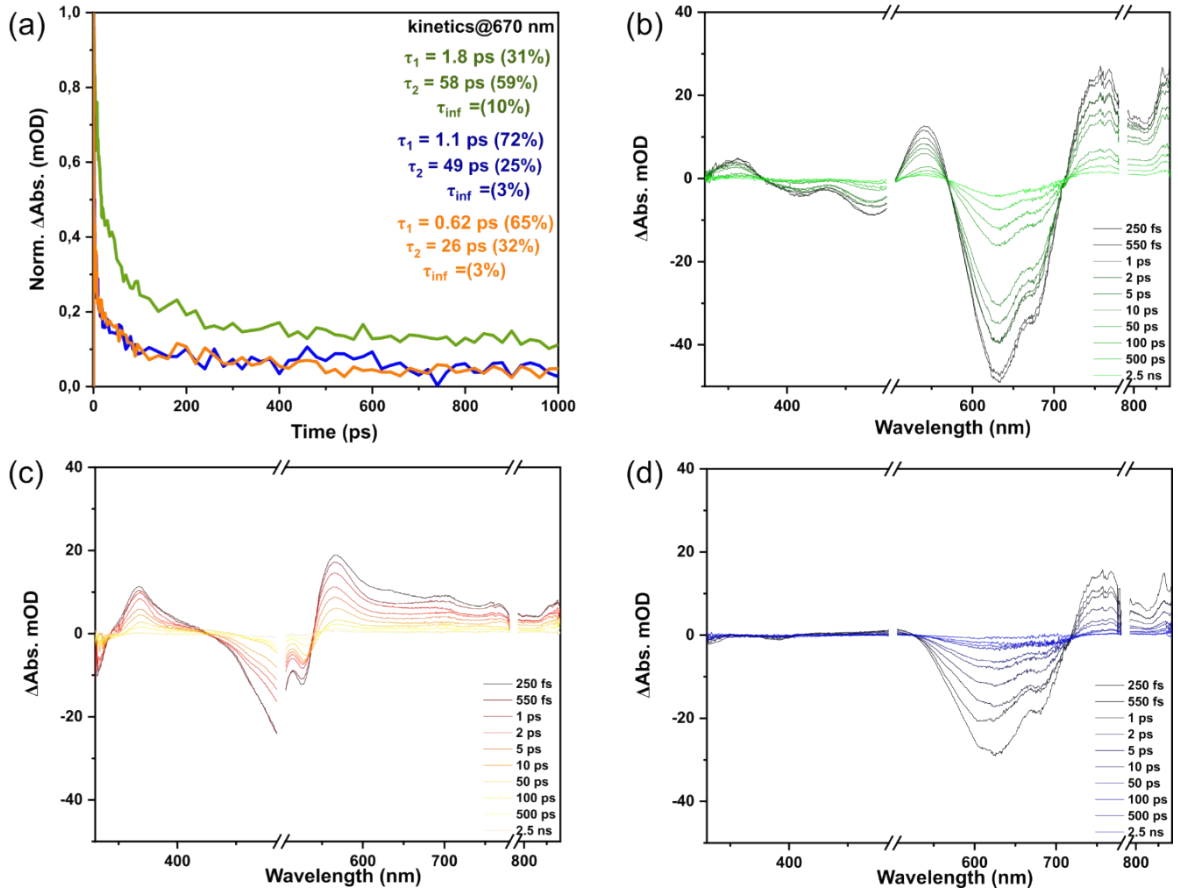

Figure S17. (a) Kinetic traces extracted at 670 nm ($\lambda_{exc.}$ 495 nm) for POZ-M:ITIC heterojunction NPs (green line), POZ-M NPs (orange line), ITIC NPs (blue line). TA data for POZ-M:ITIC NPs (b), POZ-M NPs (c) and ITIC NPs (d) excited at 495 nm

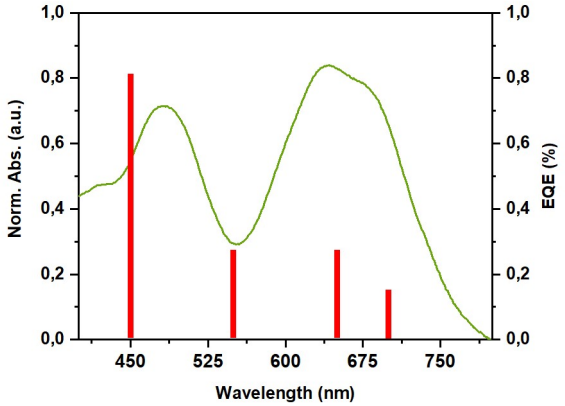

Figure S18. UV-Vis spectrum and EQYs of POZ-M:ITIC NPs for H_2 production

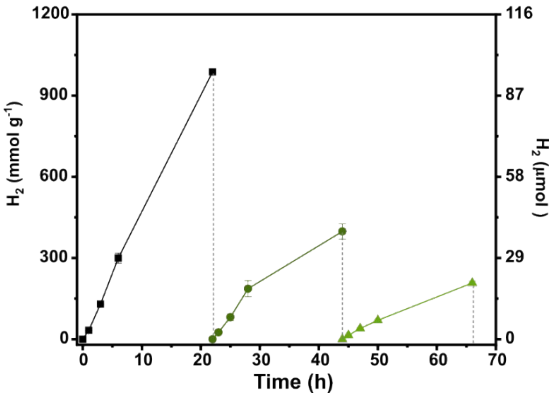

Figure S19. Recycling experiment of H_2 evolution for POZ-M:ITIC NPs (95 µg) initiated by LED irradiation (50 mW·cm^{-2}, 420-750 nm) in the presence of 6 wt% Pt, 0.2 M ascorbic acid at pH 4 (total reaction volume 2 mL).

In Figure S19, the photostability test of heterojunction NPs by removing the generated gas at a certain time revealed that the overall activity of POZ-M:ITIC NPs slightly slows down on the second day of continuous illumination, most likely due to partial photocatalyst precipitation.

Table S2. The table comparing the performance of organic photocatalysts in H_2 evolution

Material	Light source	Conditions	Activity ($\mu mol \cdot h^{-1} \cdot g^{-1}$)	EQE	Cocatalyst	Reference
Polymer based materials						
PFTFQ-PtPy5	LED (20W), λ > 420 nm	Diethylamine	4100	0.4@515 nm	Pt(5 mol. %)	[1]
PFN-Br	Xe (300W), λ > 300 nm	Triethanolamine	4280	N/A	Pt (1.5wt. %)	[2]
PFNDPP-Br	Xe (300W), λ > 300 nm	Ascorbic acid (0.2 M), pH 4	11160	0.1@550nm 0.4@600nm 0.4@650nm	Pt (3wt. %)	[2]
PFBDD-PtPy	LED (20W), λ > 420 nm	Triethylamine	960	0.3@420nm	Pt (4.9wt. %)	[3]
PF8DTBT	Xe (300W)λ (N/A)	Ascorbic acid (0.2 M), pH 4	3790	N/A	Pt (3wt. %)	[4]
PCDTBT / PC60BM	Xe (300W), λ > 420 nm	Ascorbic acid (0.2 M)	179000	3.7@420nm	Pt (3wt. %)	[5]
PTB7-Th/EH-IDTBR	Xe (300W), 350-800 nm	Ascorbic acid (0.2 M)	64426	5.6@660 nm	Pt (10wt %)	[6]
PFBT / PFODTBT/ ITIC	LED (17W), λ > 420 nm	Ascorbic acid (0.2 M), pH 4	60800	7.1@600 nm	Pt (6 wt%)	[6]
Small molecule organic photocatalyst						
P-PMDI nanobelts	λ > 400 nm	Ascorbic acid	11700	2.9@550nm	Pt (3 wt%)	[7]
RhB-C18	λ > 360 nm	Ascorbic acid (0.5 M)	3700	0.06@525nm	Pt	[8]
CNP-f	LED, λ > 420 nm	Ascorbic acid (0.04 M)	31850	2.7@490nm	Pt (3 wt%)	[9]
F1	Xe (300W), λ > 300 nm	Ascorbic acid (0.2 M)	152600	3.8@450nm 6.9@600nm	Pt (30 wt%)	[10]
Y6CO	Xe (300W), λ > 330 nm	Ascorbic acid (0.2 M)	230980	6@500nm	Pt (38 wt%)	[11]
Y6	Xe (300W),	Ascorbic acid (0.2 M)	4200	0.05@780nm	Pt (2 wt%)	[12]
Small molecule heterojunction organic photocatalyst						
POZ-M:ITIC	LED (17W), λ > 420 nm	Ascorbic acid (0.2 M), pH 4	63000	0.8@450 nm	Pt (6 wt%)	This work

References

(1) Tseng, P.-J.; Chang, C.-L.; Chan, Y.-H.; Ting, L.-Y.; Chen, P.-Y.; Liao, C.-H.; Tsai, M.-L.; Chou, H.-H. Design and Synthesis of Cycloplatinated Polymer Dots as Photocatalysts for Visible-Light-Driven Hydrogen Evolution. *ACS Catal.* **2018**, *8* (9), 7766–7772. https://doi.org/10.1021/acscatal.8b01678.

(2) Hu, Z.; Zhang, X.; Yin, Q.; Liu, X.; Jiang, X. fang; Chen, Z.; Yang, X.; Huang, F.; Cao, Y. Highly Efficient Photocatalytic Hydrogen Evolution from Water-Soluble Conjugated Polyelectrolytes. *Nano Energy* **2019**, *60*, 775–783. https://doi.org/10.1016/j.nanoen.2019.04.027.

(3) Chang, C. L.; Lin, W. C.; Jia, C. Y.; Ting, L. Y.; Jayakumar, J.; Elsayed, M. H.; Yang, Y. Q.; Chan, Y. H.; Wang, W. S.; Lu, C. Y.; Chen, P. Y.; Chou, H. H. Low-Toxic Cycloplatinated Polymer Dots with Rational Design of Acceptor Co-Monomers for Enhanced Photocatalytic Efficiency and Stability. *Appl. Catal. B Environ.* **2020**, *268*, 118436. https://doi.org/10.1016/j.apcatb.2019.118436.

(4) Zhang, X.; Shen, F.; Hu, Z.; Wu, Y.; Tang, H.; Jia, J.; Wang, X.; Huang, F.; Cao, Y. Biomass Nanomicelles Assist Conjugated Polymers/Pt Cocatalysts to Achieve High Photocatalytic Hydrogen Evolution. *ACS Sustain. Chem. Eng.* **2019**, *7* (4), 4128–4135. https://doi.org/10.1021/acssuschemeng.8b05637.

(5) Yang, H.; Li, X.; Sprick, R. S.; Cooper, A. I.; Sebastian Sprick, R.; Cooper, A. I. Conjugated Polymer Donor-Molecular Acceptor Nanohybrids for Photocatalytic Hydrogen Evolution: Conjugated Polymer Donor-Molecular Acceptor Nanohybrids for Photocatalytic Hydrogen Evolution. *Chem. Commun.* **2020**, *56*, 6790–6793. https://doi.org/10.26434/chemrxiv.11418375.v1.

(6) Kosco, J.; Bidwell, M.; Cha, H.; Martin, T.; Howells, C. T.; Sachs, M.; Anjum, D. H.; Gonzalez Lopez, S.; Zou, L.; Wadsworth, A.; Zhang, W.; Zhang, L.; Tellam, J.; Sougrat, R.; Laquai, F.; DeLongchamp, D. M.; Durrant, J. R.; McCulloch, I. Enhanced Photocatalytic Hydrogen Evolution from Organic Semiconductor Heterojunction Nanoparticles. *Nat. Mater.* **2020**, *19* (5), 559–565. https://doi.org/10.1038/s41563-019-0591-1.

(7) Kong, K.; Zhang, S.; Chu, Y.; Hu, Y.; Yu, F.; Ye, H.; Ding, H.; Hua, J. A Self-Assembled Perylene Diimide Nanobelt for Efficient Visible-Light-Driven Photocatalytic H2 Evolution. *Chem. Commun.* **2019**, *55* (56), 8090–8093. https://doi.org/10.1039/C9CC03465J.

(8) Shigemitsu, H.; Tani, Y.; Tamemoto, T.; Mori, T.; Li, X.; Osakada, Y.; Fujitsuka, M.; Kida, T. Aggregation-Induced Photocatalytic Activity and Efficient Photocatalytic Hydrogen Evolution of Amphiphilic Rhodamines in Water. *Chem. Sci.* **2020**, *11* (43), 11843–11848. https://doi.org/10.1039/D0SC04285D.

(9) Yang, H.; Li, C.; Liu, T.; Fellowes, T.; Chong, S. Y.; Catalano, L.; Bahri, M.; Zhang, W.; Xu, Y.; Liu, L.; Zhao, W.; Gardner, A. M.; Clowes, R.; Browning, N. D.; Li, X.; Cowan, A. J.; Cooper, A. I. Packing-Induced Selectivity Switching in Molecular Nanoparticle Photocatalysts for Hydrogen and Hydrogen Peroxide Production. *Nat. Nanotechnol.* **2023**, https://doi.org/10.1038/s41565-022-01289-9. https://doi.org/10.1038/s41565-022-01289-9.

(10) Zhu, Y.; Zhang, Z.; Si, W.; Sun, Q.; Cai, G.; Li, Y.; Jia, Y.; Lu, X.; Xu, W.; Zhang, S.; Lin, Y. Organic Photovoltaic Catalyst with Extended Exciton Diffusion for High-Performance Solar Hydrogen Evolution. *J. Am. Chem. Soc.* **2022**, *144* (28), 12747–12755. https://doi.org/10.1021/jacs.2c03161.

(11) Liang, Y.; Li, T.; Lee, Y.; Zhang, Z.; Li, Y.; Si, W.; Liu, Z.; Zhang, C.; Qiao, Y.; Bai, S.; Lin, Y. Organic Photovoltaic Catalyst with σ-π Anchor for High-Performance Solar Hydrogen Evolution. *Angew. Chemie Int. Ed.* **2023**, e202217989. https://doi.org/https://doi.org/10.1002/anie.202217989.

(12) Dolan, A.; M. de la Perrelle, J.; D. Small, T.; R. Milsom, E.; F. Metha, G.; Pan, X.; R. Andersson, M.; M. Huang, D.; W. Kee, T. Surfactant Effects on Hydrogen Evolution by Small-Molecule Nonfullerene Acceptor Nanoparticles. *ACS Appl. Nano Mater.* **2022**, *5* (9), 12154–12164.